Macromolecules

Article

Cite This: Macromolecules 2019, 52, 5829−5837

pubs.acs.org/Macromolecules

Application of Time-Resolved Fluorescence Anisotropy To Probe Quinoline-Based Foldamers Labeled with Oligo(phenylene vinylene)

Jingqi Wang,[†] Hunter Little,[†] Jean Duhamel,*[,†] Xuesong Li,[‡] Nagula Markandeya,[‡] Victor Maurizot,*[,‡] and Ivan Huc*[,‡,§]

[†]Institute for Polymer Research, Waterloo Institute for Nanotechnology, Department of Chemistry, University of Waterloo, 200 University Avenue West, Waterloo, Ontario N2L 3G1, Canada

[‡]Université de Bordeaux, CNRS, Bordeaux Institut National Polytechnique, CBMN (UMR 5248), Institut Europeen de Chimie Biologie, 2 Rue Escarpit, 33600 Pessac, France

[§]Department Pharmazie, Ludwig-Maximilians-Universität München, Butenandtstraße 5-13, D-81377 Munich, Germany

Supporting Information

ABSTRACT: A series of oligoquinoline carboxamides (Q_n with n = 1−32) were prepared with an oligo(phenylene vinylene) (OPV) fluorophore covalently attached at one end via a rigid amide bond. The fluorescence decays of the OPV-Q_n solutions in chloroform were acquired with a vertically polarized excitation and an emission that was either vertically or horizontally polarized to yield the fluorescence decays $I_{VV}(t)$ and $I_{VH}(t)$, respectively. The $I_{VV}(t)$ and $I_{VH}(t)$ decays were fitted globally assuming a monoexponential anisotropy. The fits were good, indicating that the theoretical triexponential anisotropy of these rigid symmetric top macromolecules was well represented by a single exponential over the range of Q_n lengths studied. The rotational time retrieved from the global analysis of the $I_{VV}(t)$ and $I_{VH}(t)$ fluorescence decays was found to increase linearly with increasing oligoquinoline chain length in agreement with the notion that these macromolecules were foldamers that adopted a rigid helical conformation in solution. Furthermore, the hydrodynamic volume of the OPV-Q_n constructs determined from their rotational times perfectly matched that expected from the known dimensions of the Q_n samples obtained from single-crystal X-ray diffraction. Unfortunately, the small aspect ratio of the foldamers prevented the resolution of the separate rotational times that would be expected from symmetric top macromolecules whose geometry could be described as ellipsoids or cylinders. Consequently, reliable values for the $D_{\parallel}$ and $D_{\perp}$ diffusion coefficients representing the tumbling of the foldamers along and perpendicular to the main axis of the symmetric top macromolecule could not be obtained for the OPV-Q_n foldamers. Nevertheless, the excellent correlation found between the foldamer size and rotational time suggests that time-resolved fluorescence anisotropy is a robust experimental technique to characterize the size and conformation of rigid foldamers in solution.

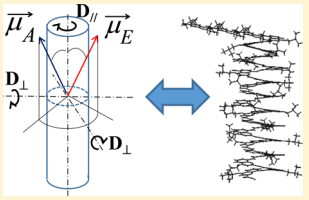

INTRODUCTION

Foldamers are artificial oligomers that are designed to fold in solution via noncovalent intramolecular interactions.[1,2] Folding of these linear molecules is inspired from natural biomolecules such as peptides, oligonucleotides, or oligosaccharides and uses comparable types of interactions to lead to similar molecular architectures such as helices, sheets, or loops. The obvious parallels that exist between foldamers and biological macromolecules in terms of conformation suggest that foldamers could be designed to perform many of the functions conducted by biological macromolecules in nature.[3,4] However and contrary to nature, chemists are not limited by the bioavailability of natural building blocks such as amino acids or nucleobases but can expand the scope of monomers used in foldamer preparation to all kinds of chemically accessible units.[5] This diversity may give access to new functions and usages remote from those commonly observed in nature, such as in molecular electronics[6−8] or in the nanoengineering field.[9−11]

In that context, foldamers based on aromatic quinoline oligoamide backbones were designed to fold into helical architectures stabilized by intramolecular hydrogen bonds and aromatic stacking.[12] Recent synthetic developments have allowed the preparation of nanometer-sized objects whose length scale and intrinsic conducting properties make them interesting as building blocks for material science applications and for molecular electronics, respectively.[11] However, these synthetic improvements also brought to the fore some obvious limitations in the choice of techniques available to characterize such large macromolecular constructs in solution. By and large, single-crystal X-ray diffraction (SCXRD) is the technique of choice to characterize the conformation of foldamers in the solid state.[13] However, crystal packing forces are also known to induce conformations in the solid state that might not be observed in solution for the same macromolecule, and

Received: March 7, 2019
Revised: June 18, 2019
Published: July 24, 2019

DOI: 10.1021/acs.macromol.9b00444
Macromolecules 2019, 52, 5829−5837

complementary solution studies are necessary.[14−16] For instance, a combination of NMR spectroscopy and molecular modeling may provide a measure of the helical twist of a foldamer that can be used to predict its conformation in solution.[17,18] Other techniques employed to assess the extent of folding of a foldamer in solution include enhanced or vibrational circular dichroism[19−21] and changes in the UV−vis absorption spectrum upon increasing foldamer length.[8,22] However, all these techniques used to probe foldamers in solution characterize short-range distances between residues in the foldamer and do not provide a sense of the overall dimension of the foldamer in solution.

The selection of a technique to probe the dimensions of foldamers in solution requires first the knowledge of the length scale to be probed. In the case of oligoquinoline foldamers, structures obtained by SCXRD indicate that these constructs adopt a helical conformation with a 2.0 nm helical diameter and a 0.136 nm raise per quinoline residue.[11] Thus, if oligoquinolines were to retain their helical conformation in solution, they would be expected to maintain a 2.0 nm diameter with a length ranging from 0.54 to 6.5 nm between a tetramer and a 48-mer construct. The technique of choice to probe nanometer-scale macromolecular objects in solution is dynamic light scattering (DLS).[23] However, most standard DLS instruments will fail to probe objects with dimensions that are less than 2 nm. Furthermore, standard DLS instruments model the objects as spheres, which would lead to errors for larger helical foldamers since such rigid symmetric top macromolecules might require two diffusion coefficients, one to handle the rotation around the main axis and another for the tumbling around the secondary axis perpendicular to the main axis. Besides DLS, Guinier plots have been obtained from small-angle X-ray scattering (SAXS) experiments conducted with a powerful high-flux synchrotron source with a solution of an *m*-phenylene ethynylene (*m*PE) octadecamer in acetonitrile.[24] The radius of gyration was found to equal 1.47 nm, which agreed with the expected structure of the folded *m*PE foldamer. While SAXS could probe the foldamer length scale at the nanometer level, the synchrotron high energy source implied that this study could not be viewed as a routine experiment, and the relatively high foldamer concentrations that were required (10^{-4}−10^{-3} M) could become an issue for less soluble foldamers. By contrast, an earlier study has established that time-resolved fluorescence anisotropy (TRFA) is ideally suited to study rigid symmetric top macromolecules with dimensions below 11 nm,[25] a range of length scales corresponding to the size of most oligoquinoline foldamers that have been prepared to date. Furthermore, these TRFA experiments took the advantage of the high sensitivity of fluorescence and were conducted at concentrations ranging between 10^{-5} and 10^{-4} M of macromolecular constructs, one order of magnitude lower than those conducted by SAXS.

Following this earlier study,[25] this report represents the first attempt to apply TRFA to probe the dimensions of foldamers in solution. To this end, a series of oligoquinolines of different sizes were synthesized and covalently labeled with an oligo(*p*-phenylene vinylene) (OPV) via a rigid amide bond to the amine terminal end to yield a series of OPV-Q_n constructs with *n* ranging from 1 to 33. The relative orientation of the OPV compared to the helix axis was fixed, almost perpendicular, and remained constant for all the tested oligomers. The TRFA experiments yielded the tumbling time of the foldamers, which was found to increase linearly with increasing foldamer length. Since the tumbling time of a macromolecule is proportional to its hydrodynamic volume, this behavior indicated that addition of a quinoline residue increased the molecular volume of the OPV-Q_n constructs by a set increment, a result in agreement with the notion that the Q_n foldamers retained their helical conformation in solution for *n* values up to 33 with a diameter and lengths in agreement with those found by SCXRD. Consequently, this study demonstrates that TRFA is reliable experimental means to probe the size of OPV-Q_n foldamers in solution, and it is expected to find numerous applications to characterize the dimensions of this fascinating family of macromolecules in solution.

EXPERIMENTAL SECTION

Materials. Chloroform (HPLC grade) was used as received in all fluorescence experiments. Except for OPV-Q_{33}, the syntheses of the other OPV-Q_n constructs terminated with a methyl ester functionality and Q_nA have been described in detail in earlier publications.[7,11] The chemical structure of the OPV-Q_n and Q_nA oligomers used in this study is presented in Figure 1. The synthesis and characterization of OPV-Q_{33} is described in the Supporting Information.

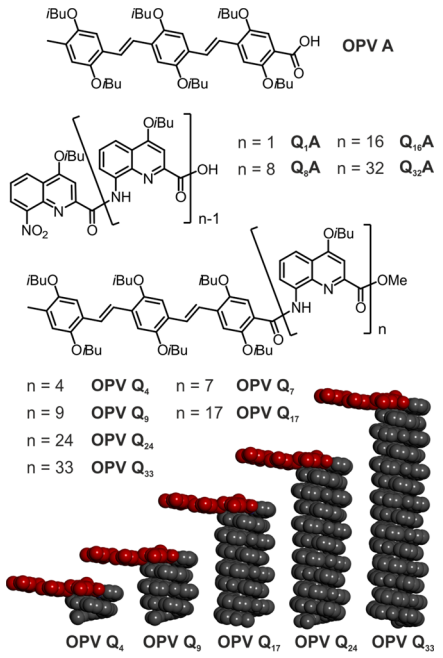

Figure 1. Chemical formula of studied oligomers and energy minimized molecular models of oligomers with the OPV unit in red to illustrate its orientation perpendicular to the helical axis. *iso*-Butoxy side chains and protons are omitted for clarity.

Absorption Measurements. Absorption spectra were acquired on a Cary 100 UV−vis spectrophotometer with quartz cells having a 1 cm path length.

Steady-State Fluorescence (SSF). Fluorescence spectra of OPV solutions in chloroform were acquired with a Photon Technology International LS-100 steady-state fluorometer using the right-angle geometry. The solutions were excited at 408 nm, and the fluorescence spectra were acquired from 420 to 700 nm.

Time-Resolved Fluorescence Anisotropy (TRFA). TRFA measurements were conducted with a HORIBA Ultima Ultrafast Fluorescence Lifetime spectrofluorometer equipped with a delta diode laser having a maximum emission intensity at 479 nm to selectively excite the OPV fragment of the OPV-Q_n foldamers (see Figure 2). The fluorescence decays were acquired with a picosecond photon detection (PPD) module model 650 using a 495 nm cutoff filter to

DOI: 10.1021/acs.macromol.9b00444
Macromolecules 2019, 52, 5829−5837

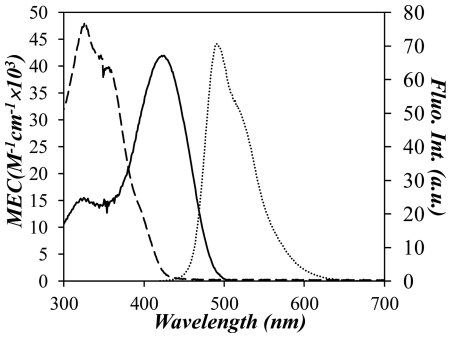

Figure 2. Spectra of the molar extinction coefficient of Q_8A (dashed line) and OPVA (solid line) and fluorescence of OPVA (dotted line) in chloroform. Conditions for the fluorescence spectrum: [OPVA] = 2.6×10^{-6} mol·L^{-1} and λ_{ex} = 408 nm.

minimize scattered light from reaching the detector. The fluorescence intensity was controlled with neutral density filters, and the slit width of the emission monochromator was set at 12 nm. The instrument response function was collected by monitoring the light reflected by a metal mirror at $\lambda_{em} = \lambda_{ex}$ = 479 nm without a 495 nm cutoff filter. All fluorescence decays were measured with a time per channel (TPC) of 12.8 ps/ch over 4096 channels except for those of the OPVA molecule whose shorter rotational time of 270 ps required a TPC of 1.37 ps/ch for more accurate analysis. For each OPV-Q_n sample, a small amount of OPV-Q_n was dissolved and diluted in chloroform to obtain an absorbance at 479 nm of 0.09 optical density corresponding to an OPV-Q_n concentration of 1.4×10^{-5} M assuming a molar extinction coefficient at 479 nm of 6250 M^{-1}·cm^{-1} for OPV bound to the foldamers (see Results and Discussion section). The fluorescence decays were acquired using an excitation light that was vertically polarized (V) and with the emission polarizer oriented at the magic angle ($I_{VM}(t)$), parallel ($I_{VV}(t)$), and perpendicular ($I_{VH}(t)$) to the vertically polarized excitation light. The analysis for a TRFA experiment began by fitting, with a single exponential, the fluorescence decay of the dye acquired with the excitation and emission polarizer sets in the vertical and magic angle (54.7°) orientations, respectively. The magic angle orientation used for the $I_{VM}(t)$ decay eliminates polarization effects.[26] All fluorescence decays were acquired with 10,000 and 20,000 counts at the decay maximum. The fit of the $I_{VM}(t)$ decays yielded a natural lifetime (τ_o) of 1.6 ns for the OPV. The vertically ($I_{VV}(t)$) and horizontally ($I_{VH}(t)$) polarized fluorescence decays are fitted to eqs 1 and 2, respectively.

$$I_{VV}(t) = \frac{I_o}{3} e^{-t/\tau_o} \times (1 + 2r(t)) \quad (1)$$

$$I_{VH}(t) = \frac{I_o}{3G} e^{-t/\tau_o} \times (1 - r(t)) \quad (2)$$

In eqs 1 and 2, G is the G-factor for TRFA measurements, and $r(t)$ represents the TRFA.[26] Contrary to classic experimental setups for TRFA measurements where the emission polarizer is flipped at set times between the vertical and horizontal positions, eqs 1 and 2 make it clear that the G-factor is only a scaling factor, which needs to be optimized in the global analysis of the fluorescence decays. This observation implies that the intensity of the excitation source, which must be carefully monitored in classic TRFA measurements that require the determination of the G-factor, becomes irrelevant in a global analysis of the $I_{VV}(t)$ and $I_{VH}(t)$ fluorescence decays where the G-factor is a scaling factor to be optimized. The advantage of this approach is that it does away with the tedious and time-consuming alternation of polarizer orientations so that both decays could be acquired with the same number of counts at the decay maximum to maximize the signal-to-noise ratio, something that is inherently impossible to achieve with the standard procedure. Additional experimental details about this procedure can be found in the Supporting Information. The TRFA could be approximated by a sum of exponentials as shown in eq 3.

$$r(t) = r_o \times \sum_{i=1}^{n} a_i \times e^{-t/\phi_i} \quad (3)$$

In eq 3, r_o is the anisotropy at time t = 0, and a_i and ϕ_i represent the ith normalized preexponential factor and rotational time of the macromolecule, respectively. All $I_{VV}(t)$ and $I_{VH}(t)$ decays could be fitted satisfyingly for all constructs with a single rotational time (n = 1 in eq 3), and the program written in house for this purpose was aniso01c. The $I_{VV}(t)$ and $I_{VH}(t)$ decays acquired with 20,000 counts at the decay maximum were also fitted using a triexponential TRFA, and the program used for this analysis was aniso02n-3. Global analysis of the polarized fluorescence decays $I_{VV}(t)$ and $I_{VH}(t)$ according to eqs 1 and 2 yielded good fits with a χ^2 parameter being smaller than 1.3 and the residuals and autocorrelation of the residuals being evenly distributed around zero. All parameters retrieved from the analysis of the fluorescence decays are listed in Tables S1 and S2 in the Supporting Information. Each TRFA measurement was conducted in triplicate to assess the error in the rotational times.

The rotational time of the OPV-labeled foldamers could then be related to the hydrodynamic volume of the macromolecule according to eq 4, where k_B is Boltzmann's constant, T is the absolute temperature, η is the solution viscosity, and V_h represents the hydrodynamic volume of the foldamer. It must be stated at this stage that strictly speaking, eq 4 should only be used for spherical objects, which the OPV-labeled foldamers were not. Nevertheless, it was found to satisfyingly describe these constructs over the range of foldamer lengths studied, and it was used as an empirical expression to describe the rotational time of the foldamers.

$$\phi = \frac{\eta \times V_h}{k_B T} \quad (4)$$

Approximating the shape of the foldamer to a cylinder implied that V_h would be a function of the squared hydrodynamic radius (R_h^2) of the cylinder, which is a constant, the height of the foldamers, which is related to the foldamer number of units (NU), the helical rise per quinoline residue (Δh), and the volume (V_o) of the OPV label as shown in eq 5. Consequently, ϕ was expected to increase linearly with increasing number of quinoline units (NU) when the temperature and viscosity of the solution remained constant.

$$\phi = \frac{\eta}{k_B T} \times (V_o + \pi R_h^2 \times \Delta h \times \mathrm{NU}) \quad (5)$$

Since Δh is known to equal 0.136 nm based on a pitch of 0.34 nm for an oligoquinoline helix containing 2.5 quinolines per helical turn, eq 5 implies that a plot of ϕ versus NU should yield a straight line if the OPV-labeled foldamers adopted a rigid helical conformation in solution.

RESULTS AND DISCUSSION

This study aimed to apply TRFA to characterize the size of a series of oligoquinoline carboxamides in solution. The chromophore OPV was rigidly attached onto the foldamers via an amide bond so that its tumbling in solution probed by TRFA closely reflected that of the foldamers. Since the absorbance of the oligoquinoline backbone overlapped that of OPV, the excitation and emission wavelengths that were employed in the TRFA measurements needed to be carefully selected.

Absorption and Fluorescence Spectra. The spectra for the molar extinction coefficient (MEC) of Q_8A (dashed line) and OPVA (solid line) and the fluorescence of OPVA are shown in Figure 2. The absorption and fluorescence spectra of oligoquinoline and OPVA match those reported in the literature.[7] Although the molar extinction coefficient of

DOI: 10.1021/acs.macromol.9b00444
Macromolecules 2019, 52, 5829−5837

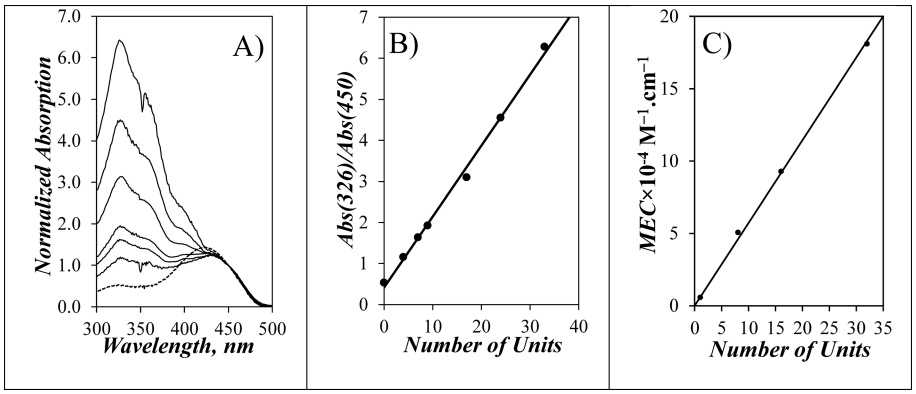

Figure 3. (A) Absorption spectra normalized at 450 nm. Bottom to top: OPVA (dashed line) and OPV-Q_4, OPV-Q_7, OPV-Q_9, OPV-Q_{17}, OPV-Q_{24}, and OPV-Q_{33}. (B, C) Plots of (B) the Abs(326 nm)/Abs(450 nm) ratio and (C) the molar extinction coefficient at 326 nm for the Q_1A, Q_8A, Q_{16}A, and Q_{32}A foldamers as a function of the number of quinoline units.

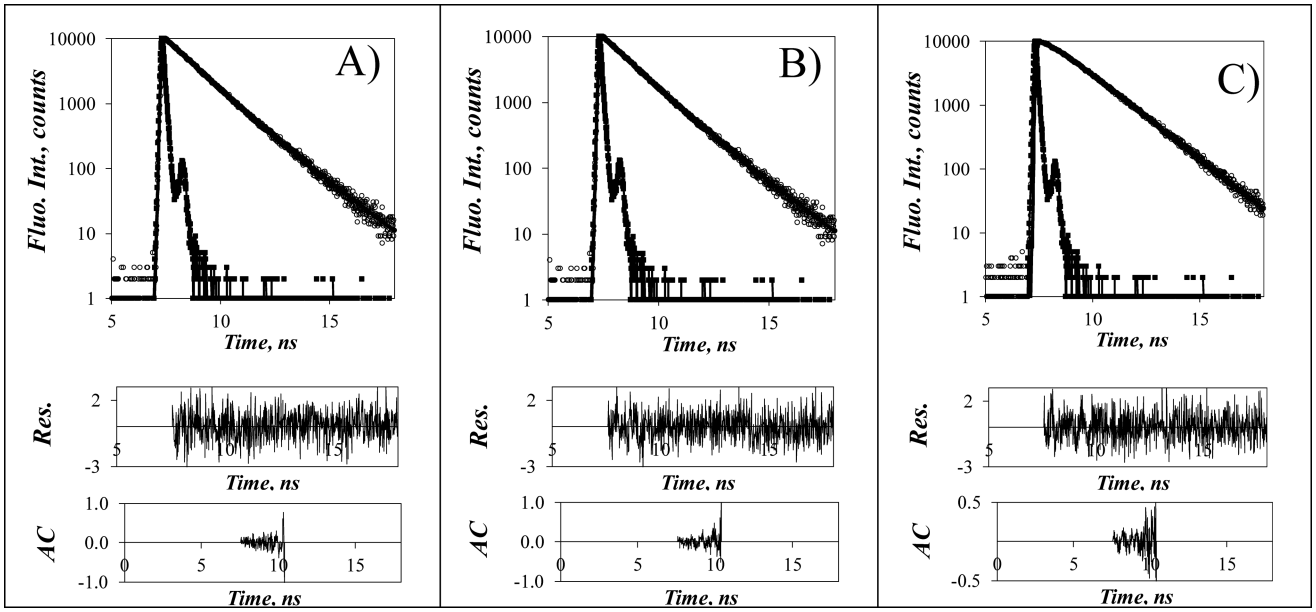

Figure 4. Global analysis of the (A) $I_{VM}(t)$, (B) $I_{VV}(t)$, and (C) $I_{VH}(t)$ fluorescence decays of OPV-Q_{33} with eqs 1 and 2. λ_{ex} = 479 nm, λ_{em} = 510 nm, χ^2 = 1.16.

OPVA passes through a maximum at 430 nm, the oligoquinoline backbone exhibits residual absorption at this wavelength. To avoid any complication, all fluorescence decays were acquired with a 479 nm excitation wavelength, and the fluorescence was collected at 510 nm. This wavelength selection ensured that the excitation photons would solely target the OPV fluorophore while yielding a strong enough fluorescence signal regardless of the quantity of oligoquinoline foldamer present in the solution.

Based on their chemical composition shown in Figure 1, the absorption of the OPV-Q_n foldamers should show a linear increase in the relative absorption of the oligoquinoline backbone with respect to that of OPV when plotted as a function of the number of units (NU) of the foldamers. This is indeed observed in Figure 3A for the OPV-Q_n foldamers where the absorption spectra were normalized to a value of unity at 450 nm where only OPVA absorbs (see Figure 2). The relative absorption of the oligoquinoline backbone was found to increase with increasing foldamer length. This trend was better illustrated by plotting the ratio of the absorbance at 326 nm over that at 450 nm, namely, the Abs(326 nm)/Abs(450 nm) ratio as a function of the number of quinoline units in Figure 3B. The linear trend obtained in Figure 3B is predicted by eq 6 where ε_{OPV}(326 nm), ε_Q(326 nm), and ε_{OPV}(450 nm) are the molar extinction coefficient (MEC) of the OPV moiety at 326 nm, one quinoline moiety at 326 nm, and the OPV moiety at 450 nm, respectively. The MEC of one quinoline moiety was determined experimentally by plotting in Figure 3C the MEC at 326 nm (ε_{QnA}(326 nm)) of the Q_1A, Q_8A, Q_{16}A, and Q_{32}A foldamers, which were available in larger quantities, as a function of the number of quinoline units. A linear relationship was obtained with a slope of 5600 ± 130 $M^{-1}\cdot cm^{-1}$, a value consistent with ε_Q(326 nm) of Q_1 found to equal 5840 (±100) $M^{-1}\cdot cm^{-1}$.

$$\frac{\text{Abs}(326\text{ nm})}{\text{Abs}(450\text{ nm})} = \frac{\varepsilon_{OPV}(326\text{ nm})}{\varepsilon_{OPV}(450\text{ nm})} + \text{NU} \times \frac{\varepsilon_Q(326\text{ nm})}{\varepsilon_{OPV}(450\text{ nm})} \quad (6)$$

The intercept of the line in Figure 3B was found to equal 0.41 (±0.09), which is comparable within the experimental error to the ε_{OPV}(326 nm)/ε_{OPV}(450 nm) ratio used in eq 6

DOI: 10.1021/acs.macromol.9b00444
Macromolecules 2019, 52, 5829−5837

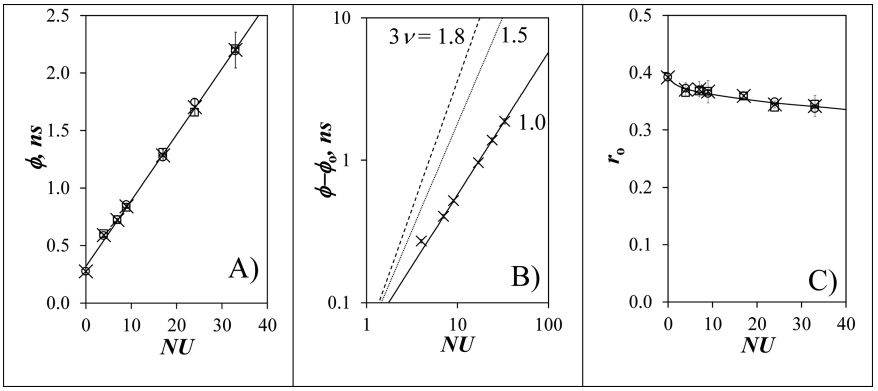

Figure 5. (A) Plot of the rotational times determined by TRFA as a function of the number of quinoline units constituting a foldamer. (B) Log−log plot of $\phi-\phi_o$ as a function of the number of units. 3ν = 1.0 (solid line), 3ν = 1.5 (dotted line), 3ν = 1.8 (dashed line). (C) Plot of r_o as a function of the number of quinoline units in the OPV-labeled foldamers. Results from the decays acquired with 10,000 (circle open) and 20,000 (box) counts and fitted with average of all ϕ and r_o values (cross mark).

found to equal 0.52 for OPVA. The slope (m) of the straight line in Figure 3B equaled 0.173 (±0.005). According to eq 6, dividing ε_Q(326 nm) by m should yield ε_{OPV}(450 nm). The ratio of ε_Q(326 nm)/m equaled 32,400 (±750) $M^{-1}\cdot cm^{-1}$, which was consistent with the MEC value of 29,300 $M^{-1}\cdot cm^{-1}$ at 450 nm for OPVA. However, since an MEC value of 32,400 (±750) $M^{-1}\cdot cm^{-1}$ was obtained for the OPV bound to the foldamers, it is this value and not that of 29,300 $M^{-1}\cdot cm^{-1}$ found for OPVA that was used to calculate the concentration of OPV-labeled foldamers by UV−vis absorption.

Time-Resolved Fluorescence Anisotropy. For each solution of 1.4×10^{-5} M OPV-labeled foldamer in chloroform, a set of three fluorescence decays were acquired with the excitation light polarized vertically and the emission polarizer oriented at the magic angle, vertically, and horizontally to obtain the $I_{VM}(t)$, $I_{VV}(t)$, and $I_{VH}(t)$ fluorescence decays, respectively. Figure 4 presents the three decays for OPV-Q_{33} as an example. The fits were good yielding low χ^2 values (<1.3) and randomly distributed residuals and autocorrelation of the residuals.

Global analysis of the $I_{VV}(t)$ and $I_{VH}(t)$ fluorescence decays according to eqs 1 and 2, respectively, yielded the rotational time (ϕ) of the OPV-labeled foldamers. Figure 5 shows a plot of ϕ as a function of the number of units (NU) in the foldamer. Within the experimental error, all ϕ values clustered around a straight line as predicted by eq 5. The intercept ϕ_o of the line with the y axis equaled 0.32 (±0.03) ns, which matched fairly closely a rotational time of 0.27 (±0.02) ns of OPVA. Consequently, the trend shown in Figure 5 indicated that the hydrodynamic volume of an OPV-labeled foldamer increased linearly with increasing number of quinoline residues. This conclusion agreed with the notion that the oligoquinoline foldamers adopted a helical conformation in chloroform, where the addition of a single quinoline residue increased the volume of the foldamer by a set increment. A similar behavior has also been reported earlier when monitoring the rotational time of a series of helical DNA duplexes as a function of the number of base pairs of the oligonucleotides.[26]

The line in Figure 5 had a slope of 0.057 (±0.001) ns. Based on the curvature of the helix, an oligoquinoline helix has 2.5 quinoline units per turn and a pitch of 0.34 nm, and each quinoline unit contributes 0.136 nm to the helix. According to these parameters, eq 5 suggests that the hydrodynamic radius of a Q_n foldamer equaled 1.01 (±0.01) nm. The radius obtained by TRFA measurements was consistent with the 1.0 nm radius of Q_n foldamers determined by SCXRD.[8]

Based on eq 4, the straight line obtained in Figure 5 implied that the volume of a Q_n foldamer was proportional to the number of its constituting quinoline units (NU). This behavior was very different from that expected from a flexible chain adopting a random coil conformation. In such a case, the volume, and thus the rotational time, of the macromolecule would increase as $NU^{3\nu}$ where ν is the Flory exponent equal to 0.5 or 0.6 in a θ or a good solvent, respectively. Regardless of whether ν equals 0.5 or 0.6, a dependency for ϕ as $NU^{3\nu}$ would result in a much steeper increase in rotational time than that shown in Figure 5B. Consequently, the linear increase observed for ϕ in Figure 4 rules out the possibility that the Q_n foldamers adopt a random coil conformation in chloroform.

Since the molar concentration of the foldamers was fixed to equal 1.4×10^{-5} M in the experiments conducted to obtain the results shown in Figure 5, the mass concentration of foldamer increased with increasing foldamer length. To ensure that the results presented in Figure 5 were not due to the aggregation of OPV-Q_n foldamers that would increase with increasing foldamer length and poorer solubility, the OPV-Q_{33} solution in chloroform was diluted up to 10-fold, and the rotational time of the foldamer was monitored as a function of concentration. As can be seen in Figure S2 in the Supporting Information, the rotational time of the foldamer remained constant with foldamer concentration demonstrating the absence of aggregation for the solutions investigated.

Finally, the r_o values corresponding to the anisotropy at $t = 0$ were plotted as a function of NU in Figure 5C for OPVA and the ester-terminated OPV-Q_n foldamers. The largest r_o value that can be obtained for any dye is 0.4. An r_o value of 0.4 indicates that the absorption and emission dipole moments of the dye are parallel. The r_o value of OPV equaled 0.39 (±0.01), a value close to 0.4, reflecting parallel absorption and emission dipole moments of OPV in agreement with earlier reports that also state that both dipole moments are aligned along the main OPV axis.[27,28] As NU increased, r_o decreased slightly indicating a loss of the initial orientation of the dipole moments that occurred on too short a time scale to be probed by the fluorometer. This rapid reorientation was probably the result of wobbling of the OPV moiety with respect to the helical foldamer. For short n values, the tumbling of the OPV-Q_n

DOI: 10.1021/acs.macromol.9b00444
Macromolecules 2019, 52, 5829−5837

foldamer in solution is determined by the tumbling of the OPV moiety. However, as n increases, it is the foldamer that dictates the tumbling of the OPV whose wobbling can no longer be transmitted to the entire macromolecule. As a result, the reduction in r_o is believed to reflect some residual loss in the rigidity of the foldamer with increasing chain length.

Anisotropy for Rigid Symmetric Top Macromolecules. The trend shown in Figure 5 between the rotational time (ϕ) and the number of units (NU) of the OPV-Q_n constructs clearly indicated that the progressive addition of quinoline units onto OPV increased the rotational time in a stepwise manner by relating the increase in ϕ to a commensurate increase in volume of the oligoquinoline foldamer. Yet, the simplicity of this result would appear somewhat fortuitous in view of the complex geometry of the OPV-Q_n foldamers. Indeed, helical foldamers are symmetric top macromolecules whose TRFA is best described by the triexponential function given in eq 7.[29]

$$\begin{aligned} r(t) = {} & 0.3 \sin^2(\beta_A) \sin^2(\beta_E) \cos(2\xi)\exp[-(4D_{\parallel} + 2D_{\perp})t] \\ & + 0.3 \sin(2\beta_A) \sin(2\beta_E) \cos(\xi) \\ & \times \exp[-(D_{\parallel} + 5D_{\perp})t] + 0.1 \times [3 \cos^2(\beta_A) - 1] \\ & \times [3 \cos^2(\beta_E) - 1] \times \exp[-6D_{\perp}t] \end{aligned} \tag{7}$$

A representation of the different parameters used in eq 7 is provided in Figure 6 for the three most common symmetric top macromolecules (oblate and prolate ellipsoids and cylinder). The angles β_A and β_E in Figure 6 represent the angles between the absorption and emission dipole moments of the dye with the main axis of the helix, respectively, while the angle ξ corresponds to the angle between the projection of the absorption and dipole moments to the plane perpendicular to the main axis of the symmetric top macromolecule. The tumbling of the dye solidly bound to the macromolecule in solution results in a triexponential TRFA whose three rotational times are a function of the two diffusion coefficients $D_{\parallel}$ and $D_{\perp}$.[25,26,29−31] Rotation around the main axis is handled by $D_{\parallel}$ while $D_{\perp}$ characterizes the tumbling of the symmetric top macromolecule around the secondary axis of the helix that is perpendicular to the main axis.

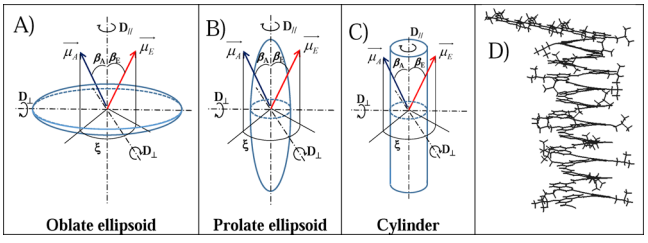

Figure 6. (A−C) Geometries for (A) an oblate ellipsoid, (B) a prolate ellipsoid, and (C) a cylinder. (D) Structure of OPV-Q_{24} determined by energy minimization with HyperChem.

Since eq 7 predicts that three different rotational times, namely, $\phi_1 = (4 \times D_{\parallel} + 2 \times D_{\perp})^{-1}$, $\phi_2 = (D_{\parallel} + 5 \times D_{\perp})^{-1}$, and $\phi_1 = (6 \times D_{\perp})^{-1}$, are required for the TRFA of symmetric top molecules, the excellent fits obtained through the global analysis of the $I_{VV}(t)$ and $I_{VH}(t)$ decays with eqs 1 and 2 using a monoexponential TRFA would suggest a problem with the analysis. This apparent contradiction, however, could be reconciled by representing the diffusion coefficients $D_{\parallel}$ and $D_{\perp}$ as a function of NU in Figure 7 for two types of ellipsoids (Ellipsoid-I and Ellipsoid-II) and a cylinder along with the corresponding decay times τ_1, τ_2, and τ_3 that would be obtained in the expressions of $I_{VV}(t)$ and $I_{VH}(t)$ in eqs 1 and 2 if the TRFA took the form of eq 7.

The calculation of the diffusion coefficients $D_{\parallel}$ and $D_{\perp}$ in Figure 7 required the dimensions of the object along the vertical and horizontal axes referred to as L and d for the length and diameter, respectively. If the macromolecular object was well described by a cylinder, as would be expected from the helical oligoquinoline foldamers, L would be represented by the product NU × Δh where NU is the number of units constituting the foldamer and Δh is the helical rise per quinoline residue equal to 0.136 nm, and d would be the helix diameter estimated to equal 2.0 nm. The aspect ratio ($p = L/d$) is the most important parameter to calculate the diffusion coefficients describing the rotation of a symmetric top macromolecule around its one vertical ($D_{\parallel}$) and two horizontal ($D_{\perp}$) axes of symmetry. As shown hereafter, the diffusion coefficients take different expressions depending on the type of symmetric top macromolecule considered in Figure 6.

In the case of an ellipsoid, the diffusion coefficients $D_{\parallel}$ and $D_{\perp}$ are given by eqs 8 and 9, respectively.[26]

$$D_{\parallel} = \frac{3p(p - S)}{2(p^2 - 1)} \times \frac{k_B T}{6\eta V_h} \tag{8}$$

$$D_{\perp} = \frac{3p[(2p^2 - 1)S - p]}{2(p^4 - 1)} \times \frac{k_B T}{6\eta V_h} \tag{9}$$

In eqs 8 and 9, k_B, T, η, and V_h are the Boltzmann constant (1.38×10^{-23} J·K^{-1}), the absolute temperature in kelvin, the solvent viscosity equal to 0.536 mPa·s for chloroform at 25 °C, and the hydrodynamic volume of a sphere of volume equivalent to that of the ellipsoid, respectively. S is a function of p whose expression given in eqs 10 and 11 depends on whether the ellipsoid is an oblate ($p < 1$) or a prolate ($p > 1$).

$$\text{For } p > 1 \text{(prolate)}, \quad S = \frac{Ln(p + \sqrt{p^2 - 1})}{\sqrt{p^2 - 1}} \tag{10}$$

$$\text{For } p < 1 \text{(oblate)}, \quad S = \frac{\arctan\left(\frac{\sqrt{1 - p^2}}{p}\right)}{\sqrt{1 - p^2}} \tag{11}$$

Two types of ellipsoids were considered for the calculation of $D_{\parallel}$ and $D_{\perp}$. Ellipsoid-I would have dimensions along the long and short axes given by L and d representing the helix length (NU × Δh) and diameter (2.0 nm), respectively. The volume of Ellipsoid-I with its round tips would thus be smaller than that of a cylinder with sharp tip edges of height L and diameter d as seen in Figure 6B,C. Yet, Figure 5 suggests that the hydrodynamics of the OPV-Q_n foldamers are well represented by cylinders whose volume is larger than that of ellipsoids having the same L and d parameters. To account for this difference, Ellipsoid-II was considered whose dimension along the secondary axis (perpendicular to the main axis) was given by d equal to 2.0 nm, that is, the diameter of a helical Q_n foldamer, but whose length L along the main axis was calculated so that its total volume given by $(\pi/6)Ld^2$ would match that of a cylinder with an NU value equal to n. The $D_{\parallel}$ and $D_{\perp}$ parameters were plotted as a function of the number of

DOI: 10.1021/acs.macromol.9b00444
Macromolecules 2019, 52, 5829−5837

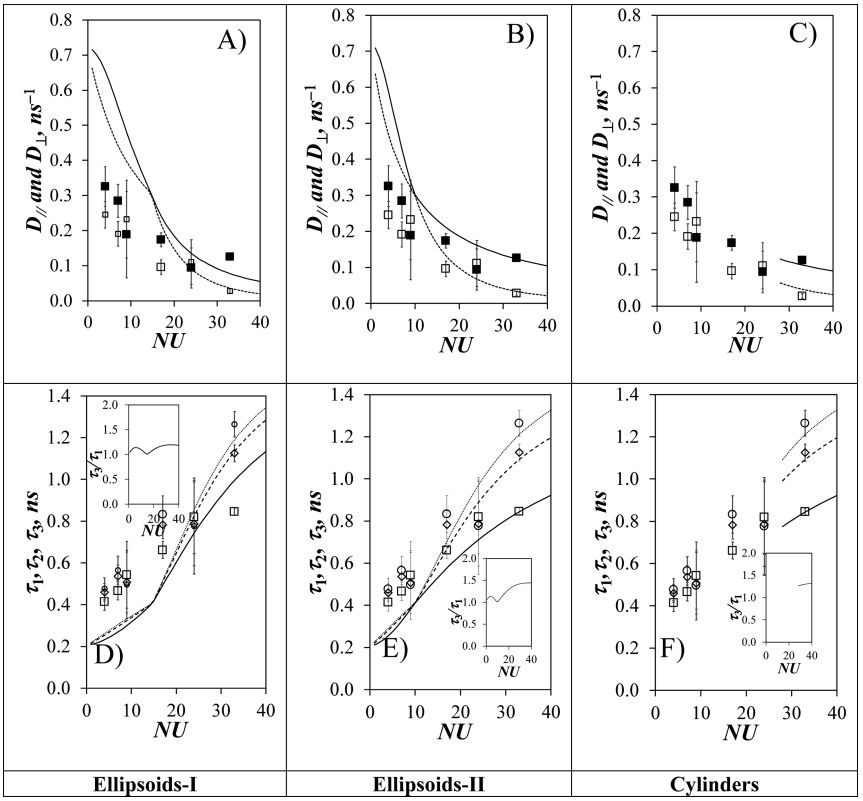

Figure 7. Plots of $D_{\|}$ (box solid, solid line) and $D_{\perp}$ (box, dashed line) as a function of the number of units for (A) Ellipsoid-I, (B) Ellipsoid-II, and (C) Cylinder. Plots of τ_1 (box, solid line), τ_2 (diamond open, dashed line), and τ_3 (circle open, dashed line) as a function of the number of units for (D) Ellipsoid-I, (E) Ellipsoid-II, and (F) cylinder. Insets represent the ratio of τ_3/τ_1 as a function of the number of units.

quinoline units in Figure 7A,B for Ellipsoid-I and Ellipsoid-II, respectively.

In the case of a cylinder, Tirado and de la Torre derived eqs 12 and 13 for $D_{\|}$ and $D_{\perp}$, respectively, for aspect ratios ($p = L/d$) of the cylinder between 2 and 30.[30]

$$D_{\|} = \frac{k_B T}{A_o \pi \eta L^3}\left(\frac{4p^2}{1 + \delta_{\|}}\right) \tag{12}$$

$$D_{\perp} = \frac{3k_B T}{\pi \eta L^3}(\ln(p) + \delta_{\perp}) \tag{13}$$

In eqs 12 and 13, A_o equals 3.814, and the functions $\delta_{\|}$ and $\delta_{\perp}$ accounting for end-effect corrections due to the cylindrical shape are given in eqs 14 and 15, respectively.[31]

$$\delta_{\|} = 1.119 \times 10^{-4} + (0.6884/p) - (0.2019/p^2) \tag{14}$$

$$\delta_{\perp} = -0.662 + (0.971/p) - (0.050/p^2) \tag{15}$$

Using $L = \mathrm{NU} \times \Delta h$ where Δh equals 0.136 nm and d equals 2.0 nm for the diameter of the cylinder, the $D_{\|}$ and $D_{\perp}$ values obtained with eqs 12−15 were plotted as a function of NU in Figure 7C. We note that eqs 12−15 are valid as long as the aspect ratio p takes a value between 2.0 and 30, which would correspond to NU values between, 28 and 441, respectively, for the oligoquinoline foldamers.

For TRF decay measurements to accurately retrieve decay times from TRF decay analysis, a commonly accepted practice is that every two decay times are separated by at least a factor of 2.[26] Incorporation of eq 7 for the TRFA into eqs 1 and 2 for the expression of the $I_{VV}(t)$ and $I_{VH}(t)$ decays would result in two tetraexponentials with one exponential being the longest component equal to the lifetime of the dye (τ_o = 1.6 ns) and whose other three decay times τ_1, τ_2, and τ_3 reporting on the rotational times ϕ_1, ϕ_2, and ϕ_3 would be represented by eqs 16−18.

$$\tau_1 = (\tau_0^{-1} + \phi_1^{-1})^{-1} = (\tau_0^{-1} + 4D_{\|} + 2D_{\perp})^{-1} \tag{16}$$

$$\tau_2 = (\tau_0^{-1} + \phi_2^{-1})^{-1} = (\tau_0^{-1} + D_{\|} + 5D_{\perp})^{-1} \tag{17}$$

$$\tau_3 = (\tau_0^{-1} + \phi_3^{-1})^{-1} = (\tau_0^{-1} + 6D_{\perp})^{-1} \tag{18}$$

The decay times τ_1, τ_2, and τ_3 were then plotted as a function of the number of quinoline units in Figure 7D−F for the Ellipsoid-I, Ellipsoid-II, and cylinder geometries, respectively. The ratio of τ_3/τ_1 between the largest and the shortest decay times was calculated for each geometry and plotted in the inset of Figure 7D−F. To properly resolve the three decay times τ_1, τ_2, and τ_3, the ratio of τ_3/τ_1 would have to be larger than 4 to ensure that τ_2/τ_1 and τ_3/τ_2 be both greater than 2. As shown in the inset of Figure 7D−F, the ratio of τ_3/τ_1 was never greater than 1.5 for all geometries considered. This result explained why the $I_{VV}(t)$ and $I_{VH}(t)$ decays could be well fitted by assuming a monoexponential TRFA instead of the triexponential function given in eq 7 indicating that recovery of three τ_1, τ_2, and τ_3 decay times would be challenging.

Despite these poor odds, an attempt was made to improve the resolving power of the fluorescence decay analysis program by adopting the following strategy. First, the $I_{VV}(t)$ and $I_{VH}(t)$ decays were acquired with 20,000 instead of 10,000 counts at the decay maximum to improve the signal-to-noise ratio. Second, the program analyzed the $I_{VV}(t)$ and $I_{VH}(t)$ decays

DOI: 10.1021/acs.macromol.9b00444
Macromolecules 2019, 52, 5829−5837

globally, which notably improves the resolving power of the fluorescence decay analysis program.[32] Third, the program did not optimize the three rotational times ϕ_1, ϕ_2, and ϕ_3 but rather optimized the diffusion coefficients $D_{\parallel}$ and $D_{\perp}$ directly, thus reducing the number of floating parameters from three decay times to two diffusion coefficients. Fourth, the angles β_A, β_E, and ξ describing the orientation of the absorption and emission dipole moments between themselves and with respect to the frame of the helical foldamer were estimated by conducting molecular mechanics optimizations (MMOs) with HyperChem and were used to calculate the preexponential factors in eq 7, which were fixed in the analysis of the fluorescence decays. The angle ξ was set to equal zero by noting that since r_o for OPVA equals 0.4 (see Figure 5C and ref 27), the absorption and emission dipole moments of OPV are parallel, thus implying that $\beta_A = \beta_E$ in Figure 6. To determine the angle $\beta_A = \beta_E$ between OPV and the main axis of the oligoquinoline helix, the published SCXRD structure of Q_{48} was imported into the modeling program HyperChem.[11] Since the structure of Q_{48} is that of an anhydride between two Q_{24}A moieties, one-half of the dimer was deleted since the anhydride moiety induced a small bend in the helix. The OPVA was covalently attached to the N-terminal of Q_{24} in silico.[11] Energy minimization of the OPV moiety while fixing the position of all the atoms of Q_{24} yielded the structure shown in Figure 6D where $\beta_A = \beta_E$ was determined to equal 99.5°. Having determined all the angles that needed to be input into eq 7, eq 19 was obtained for the anisotropy of the OPV-Q_n foldamers.

$$r(t) = r_o \times \{0.71 \times \exp[-t \times (4D_{\parallel} + 2D_{\perp})] + 0.08 \times \exp[-t \times (D_{\parallel} + 5D_{\perp})] + 0.21 \times \exp[-t \times (6D_{\perp})]\} \quad (19)$$

The advantage of using eq 19 compared to eq 7 with three floating rotational times and three floating preexponential factors was to reduce the number of floating parameters from 6 to 3, namely, r_o, $D_{\parallel}$, and $D_{\perp}$. All $I_{VV}(t)$ and $I_{VH}(t)$ decays acquired with 20,000 counts at the decay maximum were fitted by inputting eq 19 into eqs 1 and 2. The recovered decay times τ_1, τ_2, and τ_3 and diffusion coefficients $D_{\parallel}$ and $D_{\perp}$ were plotted as a function of number of units in Figure 7. For all OPV-Q_n constructs, the τ_1, τ_2, and τ_3 decay times clustered together as would be expected from these objects having a small aspect ratio ($p < 2.2$) and as found experimentally since a single rotational time was sufficient in eq 7 to fit the $I_{VV}(t)$ and $I_{VH}(t)$ decays. Only in the case of the longest OPV-Q_{33} sample did the $D_{\parallel}$ and $D_{\perp}$ diffusion coefficients and τ_1, τ_2, and τ_3 decay times line up with the trends expected for an Ellipsoid-II or cylinder geometry. The decay times retrieved for the smaller ellipsoids representing the shorter helical foldamers were longer than expected, thus indicating longer rotational times. These longer rotational times were probably due to the 18.7 Å long and 8.7 Å wide OPV moiety as determined from MMOs conducted with HyperChem. Considering its ϕ value of 0.27 ns, OPVA would have a hydrodynamic volume of 2.1 nm^3 that is equivalent to that of a pentaquinoline foldamer. OPVA will thus slow down the diffusion of the shorter foldamers, but its effect should decrease with increasing foldamer length, becoming negligible for the longer foldamers with 20 or more oligoquinolines where the OPVA volume will represent less than 20% of the overall volume of the macromolecule.

While it is clear that the dimension of the fluorescent OPV label affects the rotational time of the OPV-Q_n foldamers, particularly for low NU, this effect is much more difficult to handle quantitatively in the case of symmetric top geometries. As it was observed in Figure 5A where the geometry of the OPV-Q_n foldamers was approximated to that of a sphere, the effect of the finite dimension of the OPV label manifested itself simply from the nonzero intercept of the straight line. Any quinoline addition contributed a set volume to the hydrodynamic volume of the OPV-Q_n foldamer resulting in the simple straight line found in Figure 5A. Although not mathematically correct, the representation of the foldamers as spherical objects appears to be fully justified for OPV-Q_n foldamers with $1 < n < 33$ based on the trends generated in Figure 7 that demonstrate that the rotational times retrieved by assuming a symmetric top geometry for these objects would result in three similar rotational times that are challenging to resolve experimentally.

CONCLUSIONS

This report has demonstrated that TRFA is ideally suited to probe the hydrodynamic behavior of rigid foldamers in solution. It was applied to a series of OPV-Q_n foldamers whose rotational time was found to increase linearly with increasing foldamer length. This result was taken as evidence that addition of one quinoline residue increased the hydrodynamic volume of the foldamer by a set amount, as would be expected from rigid helical objects. Furthermore, the hydrodynamic volume of the OPV-Q_n constructs matched perfectly that expected from the dimensions of oligoquinoline helices in the solid state retrieved from SCXRD. The excellent agreement between the structural information retrieved for the foldamers in the solid state by SCXRD and the solution by TRFA is evidence of the reliability of TRFA to probe the structure of rigid foldamers in solution. Consequently, this study opens the path to the use of TRFA in the characterization of foldamers in solution.

ASSOCIATED CONTENT

Supporting Information

The Supporting Information is available free of charge on the ACS Publications website at DOI: 10.1021/acs.macromol.9b00444.

Synthesis and characterization of OPV-Q_{33} and parameters retrieved from the fluorescence decay analysis (PDF)

AUTHOR INFORMATION

Corresponding Authors

*E-mail: jduhamel@uwaterloo.ca (J.D.).
*E-mail: victor.maurizot@u-bordeaux.fr (V.M.).
*E-mail: ivan.huc@cup.lmu.de (I.H.).

ORCID

Jean Duhamel: 0000-0002-7575-2990
Ivan Huc: 0000-0001-7036-9696

Notes

The authors declare no competing financial interest.

ACKNOWLEDGMENTS

J.W., H.L., and J.D. thank a collaborative funding opportunity from the University of Waterloo and NSERC.

DOI: 10.1021/acs.macromol.9b00444
Macromolecules 2019, 52, 5829−5837

REFERENCES

(1) Gellman, S. H. Foldamers: A manifesto. *Acc. Chem. Res.* **1998**, *31*, 173−180.
(2) Guichard, G.; Huc, I. Synthetic Foldamers. *Chem. Commun.* **2011**, *47*, 5933−5941.
(3) Cole, J. P.; Hanlon, A. M.; Rodriguez, K. J.; Berda, E. B. Protein-Like Structure and Activity in Synthetic Polymers. *J. Polym. Sci., Part A: Polym. Chem.* **2017**, *55*, 191−206.
(4) Goodman, C. M.; Choi, S.; Shandler, S.; DeGrado, W. F. Foldamers as versatile frameworks for the design and evolution of function. *Nat. Chem. Biol.* **2007**, *3*, 252−262.
(5) Hecht, S.; Huc, I. *Foldamers: Structure, Properties and Applications*; Wiley: Weinheim, Germany, 2007.
(6) Wolffs, M.; Delsuc, N.; Veldman, D.; Anh, N. V.; Williams, R. M.; Meskers, S. C. J.; Janssen, R. A. J.; Huc, I.; Schenning, A. P. H. J. Helical Aromatic Oligoamide Foldamers as Organizational Scaffolds for Photoinduced Charge Transfer. *J. Am. Chem. Soc.* **2009**, *131*, 4819−4829.
(7) Li, X.; Markandeya, N.; Jonusauskas, G.; McClenaghan, N. D.; Maurizot, V.; Denisov, S. A.; Huc, I. Photoinduced electron transfer and hole migration in nanosized helical aromatic oligoamide foldamers. *J. Am. Chem. Soc.* **2016**, *138*, 13568−13578.
(8) Carini, M.; Ruiz, M. P.; Usabiaga, I.; Fernández, J. A.; Cocinero, E. J.; Melle-Franco, M.; Diez-Perez, I.; Mateo-Alonso, A. High Conductance Values in π−Folded Molecular Junctions. *Nat. Commun.* **2017**, *8*, 15195.
(9) Yu, Z.; Hecht, S. Cooperative Switching Events in Azobenzene Foldamer Denaturation. *Chem. − Eur. J.* **2012**, *18*, 10519−10524.
(10) Li, X.; Qi, T.; Srinivas, K.; Massip, S.; Maurizot, V.; Huc, I. Synthesis and Multibromination of Nanosized Helical Aromatic Amide Foldamers via Segment-Doubling Condensation. *Org. Lett.* **2016**, *18*, 1044−1047.
(11) Wang, X.; Wicher, B.; Ferrand, Y.; Huc, I. Orchestrating Directional Molecular Motions: Kinetically Controlled Supramolecular Pathways of a Helical Host on Rodlike Guests. *J. Am. Chem. Soc.* **2017**, *139*, 9350−9358.
(12) Jiang, H.; Léger, J.-M.; Huc, I. Aromatic δ−Peptides. *J. Am. Chem. Soc.* **2003**, *125*, 3448−3449.
(13) Zhang, D.-W.; Zhao, X.; Hou, J.-L.; Li, Z.-T. Aromatic Amide Foldamers: Structures, Properties, and Functions. *Chem. Rev.* **2012**, *112*, 5271−5316.
(14) Cheong, C.; Varani, G.; Tinoco, I. Solution Structure of an Unusually Stable RNA Hairpin, 5'GGAC(UUCG)GUCC. *Nature* **1990**, *346*, 680−682.
(15) Holbrook, S. R.; Cheong, C.; Tinoco, I., Jr.; Kim, S.-H. Crystal Structure of an RNA Double Helix Incorporating a Track of non-Watson-Crick Base Pairs. *Nature* **1991**, *353*, 579−581.
(16) Kanyo, J. E.; Duhamel, J.; Lu, P. Secondary Structure of the r(CUUCGG) Tetraloop. *Nucleic Acids Res.* **1996**, *24*, 4015−4022.
(17) Soptokova-de Olivera Santos, J.; Voisin-Chiret, A. S.; Burzicki, G.; Sebaoun, L.; Sebban, M.; Lohier, J.-F.; Legay, R.; Oulyadi, H.; Bureau, R.; Rault, S. Structural Characterizations of Oligopyridyl Foldamers, α-Helix Mimetics. *J. Chem. Inf. Model.* **2012**, *52*, 429−439.
(18) Hartley, C. S. Folding of ortho-Phenylenes. *Acc. Chem. Res.* **2016**, *49*, 646−654.
(19) Maayan, G.; Ward, M. D.; Kirshenbaum, K. Folded Biomimetic Oligomers for Enantioselective Catalysis. *Proc. Natl. Acad. Sci.* **2009**, *106*, 13679−13684.
(20) Hua, Y.; Flood, A. H. Flipping the Switch on Chloride Concentrations with a Light-Active Foldamer. *J. Am. Chem. Soc.* **2010**, *132*, 12838−12840.
(21) Buffeteau, T.; Ducasse, L.; Poniman, L.; Delsuc, N.; Huc, I. Vibrational Circular Dichroism and ab initio Structure Elucidation of an Aromatic Foldamer. *Chem. Commun.* **2006**, 2714−2716.
(22) Bornhof, A.-B.; Bauzá, A.; Aster, A.; Pupier, M.; Frontera, A.; Vauthey, E.; Sakai, N.; Matile, S. Synergistic Anion − (π)n − π Catalysis on π −Stacked Foldamers. *J. Am. Chem. Soc.* **2018**, *140*, 4884−4892.
(23) Berne, B. J.; Pecora, R. *Dynamic Light Scattering with Applications to Chemistry, Biology, and Physics*; Dover Publications: Mineola, NY, 2000.
(24) Kelley, R. F.; Rybtchinski, B.; Stone, M. T.; Moore, J. S.; Wasielewski, M. R. Solution-Phase Structure of an Artificial Foldamer: X-Ray Scattering Study. *J. Am. Chem. Soc.* **2007**, *129*, 4114−4115.
(25) Duhamel, J.; Kanyo, J.; Dinter-Gottlieb, G.; Lu, P. Fluorescence Emission of Ethidium Bromide Intercalated in Defined DNA Duplexes: Evaluation of Hydrodynamics Components†. *Biochemistry* **1996**, *35*, 16687−16697.
(26) Lakowicz, J. R. *Principles of Fluorescence Spectroscopy*, 2nd ed.; Kluwer Academic; New York, 1999.
(27) Egelhaaf, H.-J.; Lüer, L.; Tompert, A.; Bäuerle, P.; Müllen, K.; Oelkrug, D. Fluorescence Anisotropy and Rotational Diffusion of Polyene-like Molecules in Solution. *Synth. Met.* **2000**, *115*, 63−68.
(28) Schäfer, J.; Breul, A.; Birckner, E.; Hager, M. D.; Schubert, U. S.; Popp, J.; Dietzek, B. Fluorescence Study of Energy Transfer in PMMA Polymers with Pendant Oligo-Phenylene-Ethynylenes. *ChemPhysChem* **2013**, *14*, 170−178.
(29) Chuang, T. J.; Eisenthal, K. B. Theory of Fluorescence Depolarization by Anisotropic Rotational Diffusion. *J. Chem. Phys.* **1972**, *57*, 5094−5097.
(30) Tirado, M. M.; de la Torre, J. G. Rotational Dynamics of Rigid, Symmetric Top Macromolecules. Application to Circular Cylinders. *J. Chem. Phys.* **1980**, *73*, 1986−1993.
(31) Fujimoto, B. S.; Miller, J. M.; Ribeiro, N. S.; Schurr, J. M. Effects of Different Cations on the Hydrodynamic Radius of DNA. *Biophys. J.* **1994**, *67*, 304−308.
(32) Duhamel, J. Global Analysis of Fluorescence Decays to Probe the Internal Dynamics of Fluorescently Labeled Macromolecules. *Langmuir* **2014**, *30*, 2307−2324.

DOI: 10.1021/acs.macromol.9b00444
Macromolecules 2019, 52, 5829−5837